

PointNetPGAP-SLC: A 3D LiDAR-based Place Recognition Approach with Segment-level Consistency Training for Mobile Robots in Horticulture

T. Barros¹, L. Garrote¹, P. Conde¹, M.J. Coombes², C. Liu², C. Premebida¹, U.J. Nunes¹

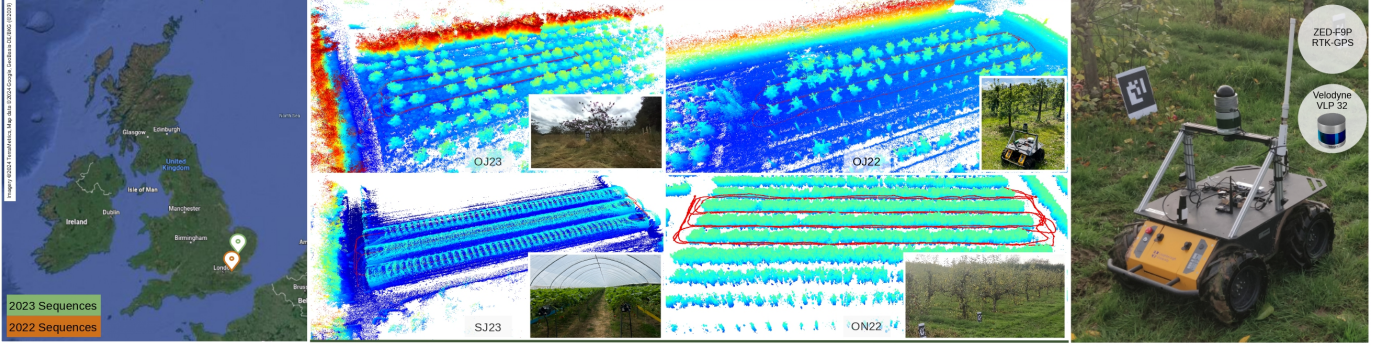


Fig. 1: Geolocation, 3D maps and recording setup of the HORTO-3DLM dataset. Four data sequences were recorded over two years at different locations in the UK, using a Husky mobile platform equipped with a 32-beam Velodyne sensor and ZED-F9P RTK GPS/GNSS system.

Abstract—This paper addresses robotic place recognition in horticultural environments using 3D-LiDAR technology and deep learning. Three main contributions are proposed: (i) a novel model called PointNetPGAP, which combines a global average pooling aggregator and a pairwise feature interaction aggregator; (ii) a Segment-Level Consistency (SLC) model, used only during training, with the goal of augmenting the contrastive loss with a context-specific training signal to enhance descriptors; and (iii) a novel dataset named HORTO-3DLM featuring sequences from orchards and strawberry plantations. The experimental evaluation, conducted on the new HORTO-3DLM dataset, compares PointNetPGAP at the sequence- and segment-level with state-of-the-art (SOTA) models, including OverlapTransformer, PointNetVLAD, and LOGG3D. Additionally, all models were trained and evaluated using the SLC. Empirical results obtained through a cross-validation evaluation protocol demonstrate the superiority of PointNetPGAP compared to existing SOTA models. PointNetPGAP emerges as the best model in retrieving the top-1 candidate, outperforming PointNetVLAD (the second-best model). Moreover, when comparing the impact of training with the SLC model, performance increased on four out of the five evaluated models, indicating that adding a context-specific signal to the contrastive loss leads to improved descriptors. The dataset and the code will be made publicly available at <https://github.com/Cybonic/PointNetPGAP-SLC.git>

I. INTRODUCTION

Autonomous robots have become more common in modern agriculture, where they have been used for various tasks such

as the application of pesticides and fertilizers, infrastructure inspection (e.g., fences and irrigation systems), and fruit and vegetable harvesting [1]. Agricultural robots require precise and accurate localization systems to operate reliably. In horticultural environments, plantations may be located within polytunnels, greenhouses or in places with lack of GNSS coverage. Therefore, in such environments, a GNSS-based localization systems may not be a reliable localization source. Alternatively, most localization systems rely on map-based approaches, where Simultaneous Localization and Mapping (SLAM) can be used to generate or update maps [2].

As part of SLAM systems, or as a standalone global localization approach, 3D LiDAR-based place recognition has seen significant advancements, driven primarily by the autonomous driving community, with the goal of achieving long-term localization [3], [4]. Despite recent efforts to adapt these methods to natural [5] and agricultural environments [6], major challenges still remain largely unresolved.

This work addresses the 3D LiDAR place recognition problem for robots operating in horticultural environments. Horticultural crops present unique challenges due to varying planting arrangements, both between different plant species and within the same species. Factors such as inter-row spacing, plant arrangement and density affect the rows' permeability to LiDAR scans, allowing beams to penetrate multiple rows. This phenomenon generates sparse and highly overlapping scans with poor geometries, which leads to inter-row descriptor ambiguity.

To cope with these challenges, we propose three key contributions:

(i) *PointNetPGAP*: A lightweight 3D LiDAR-based place recognition model that utilizes PointNet [7] for local feature

¹T.Barros, L.Garrote, P.Conde, C.Premebida and U.J.Nunes are with the University of Coimbra, Institute of Systems and Robotics, Department of Electrical and Computer Engineering, Portugal. E-mails: {tiagobarros, garrote, pedro.conde, cpremebida, urbano}@isr.uc.pt

² M.J.Coombes and C.Liu are with the Dept. of Aeronautical and Automotive Engineering, LUCAS Lab, Loughborough University, UK. E-mails:{M.J.Coombes, C.Liu5}@lboro.ac.uk

extraction and aggregates the local features by combining a global average pooling with another aggregator that explores pairwise feature interactions into a single descriptor.

(ii) *Segment-Level Consistency (SLC) model*: A model introduced during training to address the inter-row descriptor ambiguity problem. Specifically, we split the crops in various segments, and use the SLC model to provide a training signal, in addition to the contrastive loss, that differentiates scans from distinct rows/segments, even if they are highly overlapped. The SLC model consists of a Multi-layer Perceptron (MLP) which predicts the segment class for each descriptor and computes the loss based on the corresponding ground-truth. By relying on the descriptors as inputs, the SLC model is easily integrated with any place recognition model that outputs descriptors.

(iii) *Horticulture 3D Localization and Mapping (HORTO-3DLM) Dataset*: A new dataset from horticultural environments comprising data from three orchards and one strawberry plantation using a 3D LiDAR sensor and RTK-GPS mounted on a mobile platform, as shown in Fig. 1. Although, in this work, this dataset is primarily employed for place recognition, it can also be utilized for other localization and mapping tasks.

We benchmark PointNetPGAP against state-of-the-art (SOTA) models, namely OverlapTransformer [8], PointNetVLAD [9], and LOGG3D-Net [10] on the HORTO-3DLM dataset using a cross-validation evaluation protocol. The results demonstrate that PointNetPGAP offers a more effective and efficient solution compared to the aforementioned SOTA models. Furthermore, we train all models with the SLC approach and report the results both at the sequence- and segment-level. Notably, all models except OverlapTransformer exhibit performance improvements, which is primarily driven by an increase in performance in segments with higher ambiguity.

The remainder of this paper is organized as follows. In Section II, we discuss related work. Section III outlines the proposed method. The experimental evaluation and the results are presented and discussed in Section IV, while the concluding remarks are provided in Section V.

II. RELATED WORK

Place recognition has been the subject of much research over the past decade, particularly in recent years, with a focus on 3D-LiDAR approaches [3]. LiDAR sensory data has been recognized as a relevant modality to achieve robustness in place recognition, primarily due to its relative invariance to challenging variations such as different seasonal or lighting conditions, which are important in horticultural robotics.

A. 3D LiDAR-based Place Recognition

In the context of 3D LiDAR-based methods, although hand-crafted descriptors are still being used [11], Deep Learning (DL) techniques have emerged as the most prevalent choice for place modeling [3]. DL-based place recognition models can be broadly split into two main components: a local feature extraction module that maps the input scan to a local feature space, and a global feature aggregation module that aggregates the local features into a global descriptor.

As for the feature extraction module, approaches can be categorized based on how the point clouds are processed: those that extract features directly from point clouds, such as PointNetVLAD [9], and those that resort to proxy representations, such as voxels [12], [13], polar coordinates [14], or depth range images [15], [8]. Recent works such as MinkLoc3D [13], LCDNet [2], and LOGG3D-Net [10] tend to primarily use voxel-based approaches, employing sparse convolutions such as PV-RCNN [16] or 4D Spatio-Temporal ConvNets [17], which have shown higher feature extraction capabilities in urban-like environments. In this work, we resort to PointNet [18] due to its efficiency and lower computational demands (as demonstrated in Section IV-F).

Regarding aggregation strategies, most 3D LiDAR place recognition frameworks rely on first-order aggregation approaches such as NetVLAD [9], [19], [2], which computes the residuals w.r.t. to feature clusters, generalized-mean pooling (GeM) [13] or global max pooling (MAC) [20] which operate directly on the feature space. Inspired by these works, we propose an aggregation approach that combines, in a single descriptor, a first-order and a second-order aggregation approach. Specifically, we combine the global average pooling aggregator with a pairwise feature interaction aggregator into a single descriptor. We compare our hypothesis with the SOTA models LOGG3D-Net [10], PointNetVLAD [9], and OverlapTransformer [8], and show through results on real-world datasets that the combination of these two statistical-based aggregators yields higher performance than each aggregator individually and also the SOTA models.

B. Datasets

3D LiDAR-based place recognition methods have gained traction as robust and scalable global localization approaches, primarily driven by the autonomous vehicle community, which works mainly on road/city environments [3]. Works such as MinkLoc3D [13], PointNetVLAD [9], LCDNet [2], or LOGG3D-Net [10] are evaluated on urban environments, using available 3D LiDAR urban datasets such as KITTI odometry [21], MulRan [22], Oxford RobotCar [23], [9], or KITTI-360 [24].

Less studied is 3D LiDAR place recognition in field or agricultural environments. One possible reason for this is the lack of available datasets which, recently, has been partially compensated by datasets such as Wild-places [25], RELIS-3D [26], ORFD [27], TreeScope [6], or VineLiDAR [28], showing the increasing interest in such environments. Thus, given the lack of real-world data, especially in horticulture, we propose a novel dataset HORTO-3DLM that includes 3D LiDAR data of semi-structured horticulture environments, particularly from fruit trees namely apples and strawberries. The goal of HORTO-3DLM is to contribute with real-world quality data suitable to place recognition/localization in the domains related to field and agricultural robotics.

III. PROPOSED APPROACH

This section introduces the PointNetPGAP and the proposed training regime, where a traditional contrastive learning approach is combined with the proposed SLC model. Figure 2

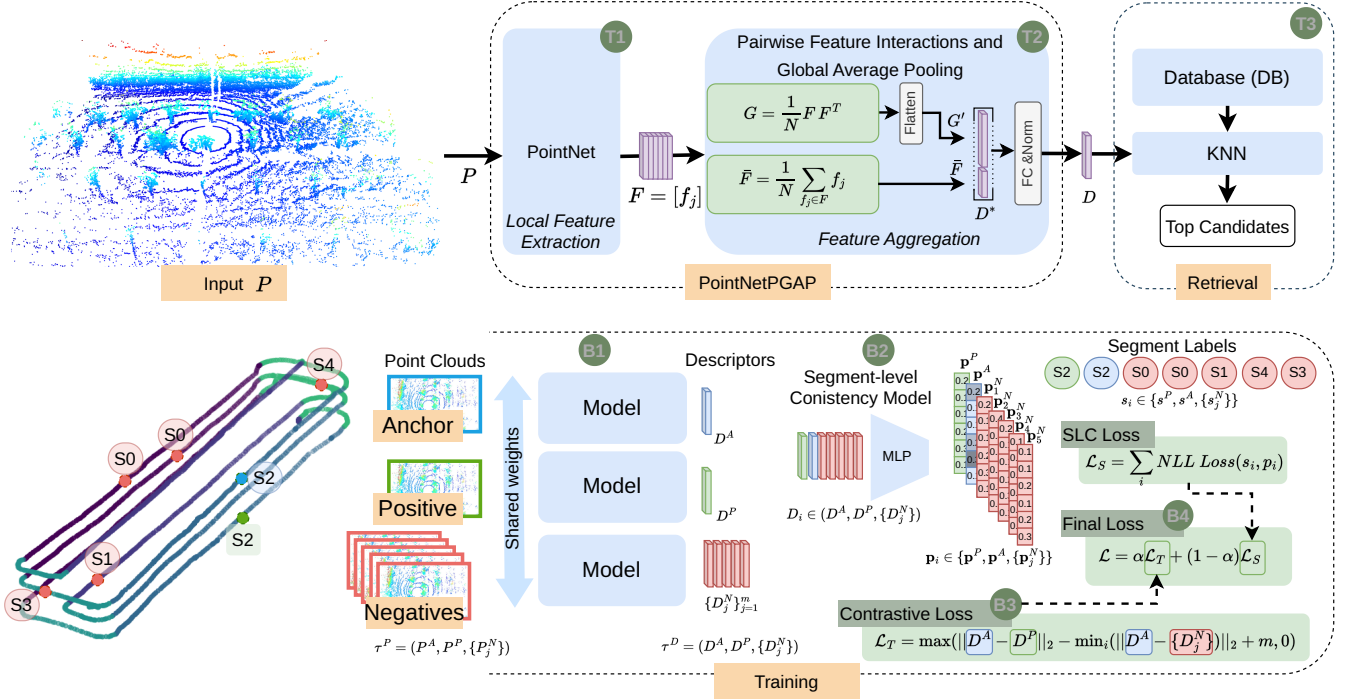


Fig. 2: **Top:** Retrieval framework using PointNetPGAP to generate global descriptors. The framework comprises the following key stages: T1) An input scan P is processed by PointNet to extract local features F ; T2) These local features are aggregated into a global descriptor D by concatenating the global average representation of local features with pairwise feature interactions into a single representation; T3) The global descriptor queries the database to retrieve the top- k most similar places. **Bottom:** Training scheme with the following stages: B1) A training tuple consisting of scans, including an anchor-positive pair and m negatives, is input into the model, which generates the corresponding descriptors; B2) In the SLC model, the descriptors are input into an MLP that predicts the corresponding segment classes. The loss is computed using the Negative Log-likelihood loss based on the predictions and ground-truth segment labels; B3) The LazyTriplet loss is calculated based on the distances between the anchor-positive pair and the anchor-negatives; B4) Finally, both losses are combined using a weight α .

outlines both PointNetPGAP in a retrieval framework (**Top**) and PointNetPGAP in the proposed training scheme (**Bottom**), with the combination of both the contrastive and the Negative Log-Likelihood (NLL) losses.

A. Problem Formulation

A retrieval-based place recognition framework comprises two stages (as illustrated in Fig. 2): firstly (denoted by T1 and T2), a LiDAR scan $P \in \mathbb{R}^{n \times 3}$ with n points is mapped to a descriptor $D \in \mathbb{R}^d$, such that $\Theta : \mathbb{R}^{n \times 3} \rightarrow \mathbb{R}^d$; then (the 2nd stage: T3), the descriptor D queries a database for the k nearest neighbors (KNN) based on a similarity metric. The k retrieved candidates represent the top- k candidates for potential revisited places. In this work, we focus on the first part (i.e., T1 and T2) and follow a retrieval framework (i.e., T3) as described in [15].

B. PointNetPGAP

PointNetPGAP, here defined as a mapping function Θ (outlined in Fig. 2 by T1, T2), can be decomposed into two functions: $\Theta \equiv \varphi \circ \phi$, where $\phi : \mathbb{R}^{n \times 3} \rightarrow \mathbb{R}^{n \times c}$ maps the input scan $P \in \mathbb{R}^{n \times 3}$ to hyper-dimensional features $F \in \mathbb{R}^{n \times c}$; and $\varphi : \mathbb{R}^{n \times c} \rightarrow \mathbb{R}^d$ aggregates the local features F into a global descriptor $D \in \mathbb{R}^d$ with d dimensions.

1) *Local Feature Extraction (T1)*: In this work, we follow the same approach as in [9] and implement ϕ based on PointNet [7], a DL-based network that operates directly on LiDAR scans. Hence, it receives a LiDAR scan $P \in \mathbb{R}^{n \times 3}$ with n points and returns a local feature representation $F \in \mathbb{R}^{n \times c}$ with c dimensions.

2) *Feature Aggregation (T2)*: As for the aggregation (i.e., φ), this work proposes the fusion of two statistically-inspired aggregators: a global average representation of the local features, also known as global average pooling, and an aggregator based on pairwise feature interactions.

The global average representation, hereafter referred to as GAP, is computed as follows:

$$\bar{F} = \frac{1}{n} \sum_{f_j \in F} f_j, \quad (1)$$

where $f_j \in \mathbb{R}^c$ represents the j -th feature point, and $\bar{F} \in \mathbb{R}^c$ represents the global average representation. As for the aggregator based on the pairwise feature interactions, it is computed using the outer product of F as follows:

$$G = \frac{1}{n} F F^T, \quad (2)$$

where $G \in \mathbb{R}^{c \times c}$ represents pairwise feature interactions of the local features, which is flattened to form a vector

representation $G' \in \mathbb{R}^{c^2}$. Finally, to create the final descriptor D , both representations are concatenated into a single vector $D^* = [G', \bar{F}] \in \mathbb{R}^{c+c^2}$, which is fed to a full-connected layer $FC: \mathbb{R}^{c+c^2} \rightarrow \mathbb{R}^d$, and normalized using the L_2 -norm:

$$D = L_2\text{-norm}(FC(D^*)). \quad (3)$$

C. Network Training

Training PointNetPGAP involves a traditional contrastive approach using the LazyTriplet loss [9], along with the proposed SLC model. The training process is illustrated at the bottom of Fig. 2 and is divided into four main stages, labeled B1, B2, B3, and B4.

1) *Training Data (B1)*: Place recognition methods traditionally resort to contrastive learning techniques, which learn to distinguish between similar (positive pairs) and dissimilar (negative pairs) data samples. In place recognition for urban environments, positive pairs are defined only by a fixed radius, which is a sufficient condition given the scale of the trajectories and revisits in these environments. However, to perform place recognition in crops with narrow rows, the radius is a necessary but not sufficient condition. The search conditions must guarantee that the search occurs along the row and does not transgress into neighboring rows. Splitting the crops into unique segments and confining the search within the segment ensures the necessary conditions.

Hence, in this work, a positive pair refers to a pair of scans that must meet the following constraints: (1) both scans must be within a r_{th} range (in meters); (2) both scans must be from different revisits, meaning that the positive scan cannot be the immediate previous scan of the anchor; and (3) both scans must be from the same segment (see Fig. 3). Scan pairs that do not meet these three constraints belong to the set of negatives.

As such, the model is trained with tuples of scans (that satisfy the aforementioned conditions) $\tau^P = (P^A, P^P, \{P_j^N\})$ where $P^A \in \mathbb{R}^{n \times 3}$ is the anchor, $P^P \in \mathbb{R}^{n \times 3}$ is the closest positive scan *w.r.t.* P^A in the Euclidean space, while $\{P_j^N | P_j^N \in \mathbb{R}^{n \times 3}\}_{j=1}^m$ is a set of m randomly selected negatives. The scan tuple τ^P is mapped to the descriptor space (as described in Section III-B), generating the corresponding descriptor tuple $\tau^D = (D^A, D^P, \{D_j^N\})$.

2) *Segment-level consistency model (B2)*: The SLC model introduces an additional signal during training, which is more context-related than the one generated by the contrastive loss. The goal is to resolve ambiguities created by scans that are highly overlapped but belong to neighboring segments. The SLC model is framed as a classification problem, aiming to predict the segment class using the descriptors as inputs. The loss between the predictions and the corresponding ground-truth segment class $s \in [1, 2, \dots, L]$, where L is the number of segments in a sequence (as shown in Fig. 3), is computed based on the NLL Loss. Hence, given a training tuple of descriptors τ^D , and the corresponding tuple of ground-truth segment classes $\tau^S = (s^A, s^P, \{s_j^N\})$, all descriptors $D_i \in \tau^D$ are fed to an MLP to predict the corresponding segment class, such that:

$$\mathbf{p}_i = \text{MLP}(D_i), \quad (4)$$

where $\mathbf{p}_i = [p_1, p_2, \dots, p_L]$ with $p_k \in [0, 1]$ representing the segment prediction scores which are used, together with the respective ground-truth segment label $s_i \in \tau^S$, to compute the loss as follows:

$$\mathcal{L}_S = \sum_i NLL\text{Loss}(\mathbf{p}_i, s_i). \quad (5)$$

3) *Contrastive Loss (B3)*: As for the contrastive cost function, the LazyTriplet loss [9] is used. Thus, given a descriptor tuple $\tau^D = (D^A, D^P, \{D_j^N\})$ the loss is computed as follows:

$$\mathcal{L}_T = \max(d_{AP} - d_{AN} + m, 0), \quad (6)$$

where $d_{AP} = \|D^A - D^P\|_2$ is the Euclidean distance between the anchor and the positive, $d_{AN} = \min_j (\|D^A - \{D_j^N\}\|_2)$ is the Euclidean distance between the anchor and the hardest negative *i.e.*, the negative that is the closest *w.r.t.* D^A in the descriptor space, while m designates a margin value.

4) *Final Loss (B4)*: Finally, both \mathcal{L}_T and \mathcal{L}_S are combined as follows:

$$\mathcal{L} = \alpha \mathcal{L}_T + (1 - \alpha) \mathcal{L}_S, \quad (7)$$

where α is adjustable weight.

IV. EXPERIMENTAL EVALUATION

To support the experiments under realistic and challenging cross-horticultural domains, we introduce a new dataset comprising four sequences from distinct horticultural crops, including detailed annotations for ground truth evaluation. This section outlines the evaluation protocol, implementation details, and training procedures, including preprocessing steps and the architecture of the proposed approach. Additionally, quantitative metrics and qualitative retrieval results are reported, showcasing the effectiveness of the approach. Furthermore, we conduct a runtime analysis to assess the computational efficiency of the PointNetPGAP.

A. The HORTO-3DLM Dataset

For real-world deployment, it is important to capture specific conditions that may induce unique challenges in agricultural environments. For instance, complex conditions may arise due to varying field layouts (row length, row width, open field, within tunnels, etc.), which can differ from plant type to plant type and even within the same plant species. Another aspect that may present challenges is the changing appearance of the same plantation due to plant growth and flowering stages.

Hence, we created a dataset called Horticulture 3D Localization and Mapping (HORTO-3DLM)*, which was recorded in the United Kingdom over two years at different locations. The dataset includes data collected from four crops: two orchards (apples and cherries), and one strawberry plantation within polytunnels with a table-top growing system. All sequences incorporate various revisits.

The data collection process involved teleoperating a Clearpath Husky mobile robot equipped with a Velodyne VLP32 3D LiDAR (10Hz) and a ZED-F9P RTK-GPS (5Hz).

*<https://github.com/Cybonic/HORTO-3DLM.git>

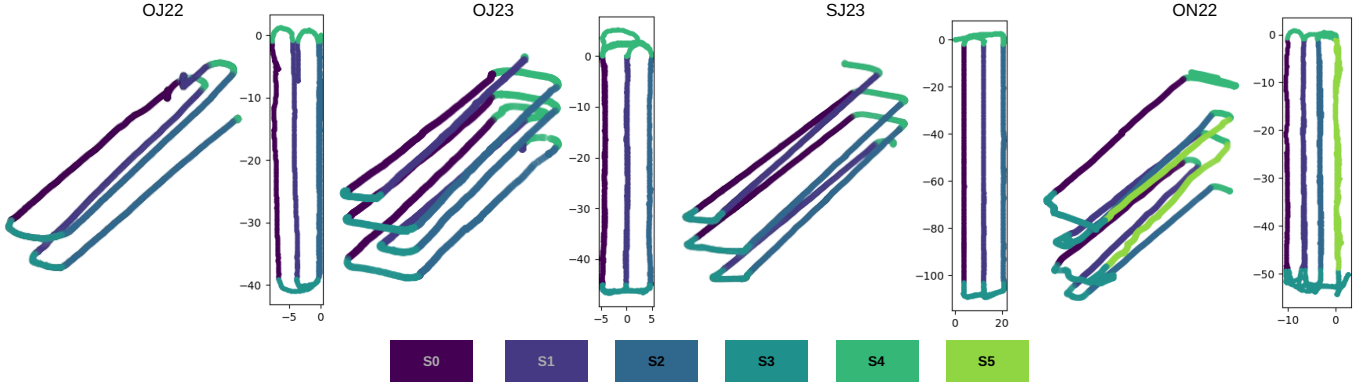


Fig. 3: 2D and 3D visualizations of the sequences' paths. The 2D representation shows the individual segments, while the 3D representation outlines the overlapping paths.

TABLE I: Summary of the four sequences. The various sequence names represent the first letter of plantation type, month and year of the recording. For example, an orchard sequence recorded in November 2022 is named ON22. The columns have the following meaning: name of the sequence (Sequence), month of recording (M), year of recording (Y), number of rows each sequence comprises (N.Rs), number of segments each sequence comprises (N.Segs), traveled distance (D) and plantation type.

Sequence	M	Y	Total Scans	N.Rs	N.Segs	D [m]	Plantation Type
Orchards							
ON22	Nov.	2022	7974	4	6	514	Apple (open)
OJ22	July	2022	4361	3	5	206	Apple (open)
OJ23	June	2023	7229	3	5	459	Cherry (open)
Strawberries							
SJ23	June	2023	6389	3	5	742	tunnels

TABLE II: Training and testing statistics used in the experiments.

Sequence	Cross-validation		
	Test Anchors	Training Anchors	Seq. Training Anchors
OJ22	1797	1605	100
OJ23	4801	1193	512
ON22	4993	1210	495
SJ23	3509	1107	598

Figure 1 showcases the geolocation, the 3D maps of the four sequences, and the recording setup mounted on the mobile robot, while Table I provides more detailed information regarding each sequence. The three sequences from orchards are denominated OJ22, ON22, and OJ23, while the sequence from the strawberry plantation is designated SJ23.

B. Methodology for Place Recognition

From the proposed HORTO-3DLM dataset described in Section IV-A, each sequence was split into various segments (S1, S2, ..., S6) as illustrated in Fig. 3. Besides the rows, we also included the extremities of the fields (*i.e.*, S3 and S4) as segments. Thus, for each data point (LiDAR scan), there exists a corresponding segment class.

Following the protocol defined in Section III-C1, r_{th} was set to 2 m for the training data, which means that a positive pair exists whenever an anchor-positive pair is within a range of 2 m. Additionally, from all anchor-positive pairs, only the anchors that were at least 0.5 m apart were selected for training. For evaluation purposes, r_{th} was set to 10 m, and all anchors were used.

C. Evaluation Protocol

The evaluation of the proposed approach is based on a k -fold cross-validation protocol, with $k = 4$, which consists of training on three sequences and testing on the sequence that was left out. This is repeated four times to obtain results on all sequences.

The dataset split for the cross-validation protocol is outlined in Table II. The entries have the following meaning: the first column (Sequence) identifies the sequence on which a given model was tested, meaning the model was trained on the remaining sequences; the second column (Test Anchors) refers to the number of anchors/loops with which the model was tested; the third column (Training Anchors) refers to the number of anchors/loops the model was trained with, corresponding to the sum of the training anchors of the remaining sequences; the fourth column (Seq. Training Anchors) refers to the number of training anchors each sequence contains individually.

As for the performance metrics, the results obtained from the proposed experiments are reported using Recall for the top- k retrieved candidates (*i.e.*, Recall@ k).

D. Training and Implementation Details

All models were trained and evaluated under the same conditions. The input scans were downsampled to 10k points,

TABLE III: Recall@1 performance of the models trained: (without SLC)/(with SLC). The bolded scores represent the highest value between trained without and with SLC, while the underling indicates the highest score in each column.

Model	OJ22	OJ23	ON22	SJ23	MEAN
OverlapTransformer [8]	0.084 /0.075 ^{-0.009}	0.153/ 0.164 ^{+0.011}	0.221 /0.194 ^{-0.027}	0.084 /0.073 ^{-0.011}	0.136 /0.127 ^{-0.009}
LOGG3D [10]	0.357/ 0.394 ^{+0.037}	0.309/ 0.329 ^{+0.020}	0.412/ 0.470 ^{+0.058}	0.254/ 0.285 ^{+0.031}	0.333/ 0.370 ^{+0.037}
PointNetVLAD [9]	0.560/ 0.659 ^{+0.099}	0.485/ 0.502 ^{+0.017}	0.611/ 0.625 ^{+0.014}	0.676/ 0.717 ^{+0.041}	0.583/ 0.630 ^{+0.043}
PNPGAP(ours)	<u>0.873</u> / 0.880 ^{+0.007}	<u>0.643</u> / 0.688 ^{+0.045}	<u>0.685</u> / 0.734 ^{+0.049}	<u>0.678</u> / 0.712 ^{+0.034}	<u>0.719</u> / 0.754 ^{+0.034}

and randomly rotated around the z-axis. The parameters of PointNetPGAP were the following: we used the original architecture of PoinNet, with T-Net disabled, descriptor size was set to 256 dimensions ($d = 256$), the local features were set to 16 dimensions ($c = 16$), the MLP was configured with three layers with 256, 64, and 6 neurons, respectively, while the weight of the final loss was set to 0.5 ($\alpha = 0.5$). The SOTA models were implemented based on the original code.

All models were trained with 200 epochs on an NVIDIA GeForce RTX 3090 GPU, using the closest positive and 20 negatives ($m = 20$) for each anchor. The margin value of the contrastive loss was set to 0.5 ($m = 0.5$), and the model parameters were optimized using the AdamW optimizer with a learning rate (L_r) of 0.0001 and a weight decay (W_d) of 0.0005. Moreover, all proposed experiments were conducted on Python 3.8, and PyTorch with CUDA 11.6.

E. Retrieval Evaluation and Discussion

This section presents and discusses the empirical results. Firstly, we conduct an ablation study on the proposed PointNetPGAP model, delineating the contribution of each aggregator to the performance. Secondly, we benchmark PointNetPGAP, both trained with and without the SLC model, against SOTA models: PointNetVLAD [9], LOGG3D-Net [10], and OverlapTransformer [8]. Each of these models adopts distinct strategies for handling scans: PointNetVLAD processes scans directly, OverlapTransformer processes scans as range images, and LOGG3D-Net relies on a voxel-based representation and network. The main results are presented in Table III and Fig. 4, while results at the segment-level are presented in Fig. 3. Furthermore, a qualitative assessment is outlined in Fig. 6. Finally, the efficiency of the models is evaluated through runtime analysis. Throughout this section, PointNetPGAP will be abbreviated as PNPGAP, and PNPGAP-SLC when trained without and with the SLC model, respectively.

1) *Ablation Study*: The results of the ablation study are reported in Table IV. For this study, we report the Recall@1 and Recall@1% of each aggregation approach separately and combined. The results indicate that combining both aggregators yields higher performance compared to each aggregator individually, improving performance by 0.6 percentage points (pp) for retrieving the Top-1% candidates and 4.7 pp for retrieving the Top-1 candidate. These results suggest that the real impact of combining these aggregation approaches is on modeling the closest neighbor.

2) *Comparison to SOTA*: PNPGAP emerges as the best model when compared to the SOTA models, outperforming PointNetVLAD (the second-best model) by 13.6 pp without

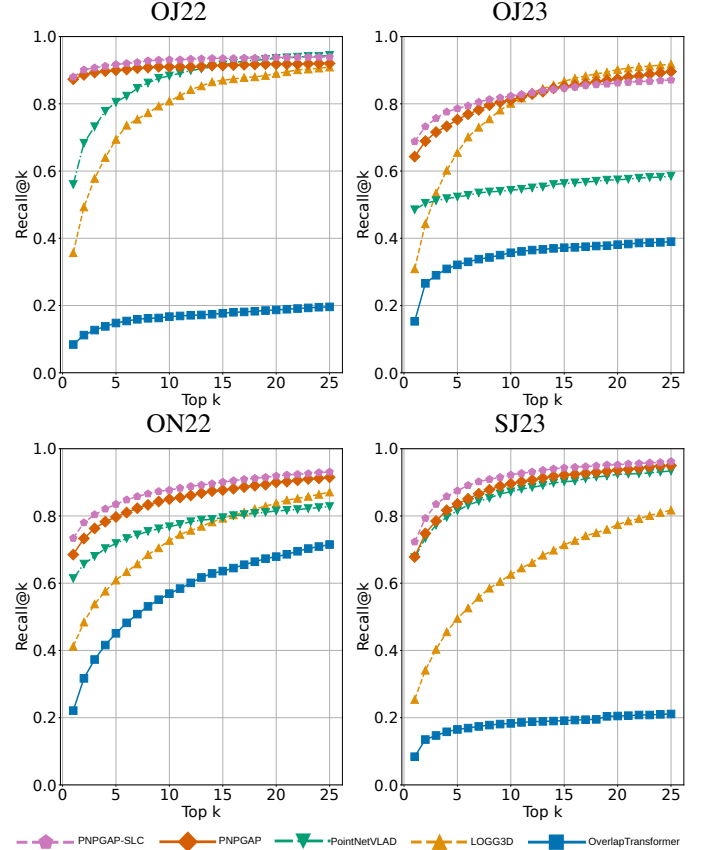


Fig. 4: Retrieval performance for the top-25 candidates on the four sequences.

TABLE IV: Ablation study of PNPGAP, where GAP represents the global average pooling aggregator and PFI represents the aggregator based on pairwise feature interactions. The bolded scores represent the highest values in each column.

GAP PFI	Recall@1					Recall@1%				
	OJ22	OJ23	ON22	SJ24	MEAN	OJ22	OJ23	ON22	SJ24	MEAN
✓	0.819	0.589	0.687	0.714	0.701	0.928	0.909	0.962	0.975	0.944
✓	0.827	0.613	0.685	0.713	0.710	0.962	0.925	0.950	0.988	0.956
✓	0.880	0.688	0.734	0.723	0.756	0.943	0.938	0.985	0.983	0.962

the SLC model and by 12.4 pp with the SLC model when retrieving the top-1 candidate. This is also evident in Fig. 6, where a qualitative assessment is shown on the paths, displaying the true positive predictions of each model when retrieving the top-1 candidate.

When analyzing the performance of retrieving the top-25 candidates (Fig. 4), LOGG3D-Net, which relies on a

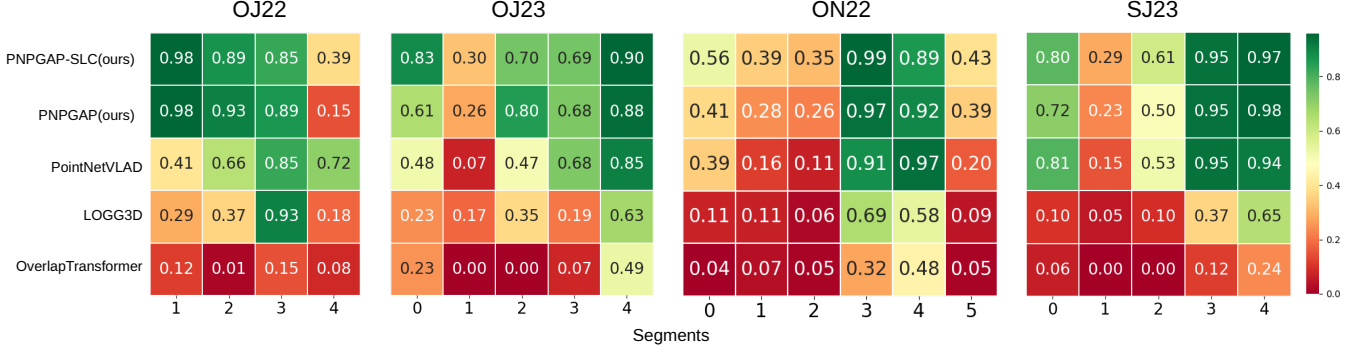


Fig. 5: Recall@1 performance at the segment-level for the four sequences. For more details on the segments, please see Fig. 3.

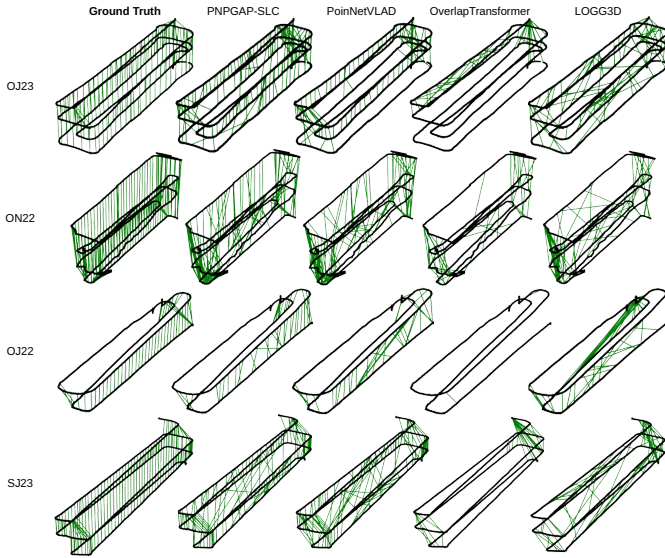


Fig. 6: True positive predictions for retrieving the top-1 candidate.

voxel-based network for feature extraction, exhibits the highest increase in performance. Meanwhile, OverlapTransformer, which relies on range images and on a CNN-based network for feature extraction, shows poor performance across all sequences. The inadequate performance of OverlapTransformer is also apparent in Fig. 6, where in some segments the model fails to predict any loops correctly. This suggests the unsuitability of this model for agricultural environments.

At the segment-level, most models perform best in segments 3 and 4, representing the extremities of the crops. As illustrated in Fig. 1, these segments are distinctive, while segments representing the rows exhibit higher similarities and thus create ambiguities among neighboring rows, resulting in lower retrieval performance.

3) *Training with the SLC Model*: The results when adding the SLC model at training time (presented in Table III) indicate that this additional training signal improves the performance throughout all sequences and models (except OverlapTransformer), with an average performance increase of 3.7 pp for LOGG3D, 4.3 pp for PointNetVLAD, and 3.34 pp for the

TABLE V: The average runtime per batch, where the batch size is 20 scans.

	Param. [M]	OJ22 [ms]	OJ23 [ms]	ON22 [ms]	SJ23 [ms]	MEAN [ms]
OverlapTransformer	48.2	12.5	11.5	11.4	11.5	11.7
LOGG3D	8.8	108.3	115.9	108.0	82.0	103.5
PointNetVLAD	19.8	23.3	22.1	22.1	22.4	22.5
PNPGAP (ours)	0.4	3.3	3.5	3.3	3.4	3.38

proposed PNP GAP model.

These findings can be further analyzed in more detail in Fig. 3, where a comparison between PNP GAP and PNP GAP-SLC is made at the segment-level. The results show that, while the performance in segments with high performance remains mostly unchanged, segments such as those corresponding to rows (*i.e.*, 1, 2, and 5) increase performance, indicating that the SLC model produces better descriptors that are less susceptible to ambiguities.

F. Runtime Analysis

The processing capacity and model size are crucial factors for real-world implementation, particularly in resource-constrained robotics applications. Throughout the runtime experiment, the results presented in Table V were obtained using identical hardware specifications as detailed in Section IV-D: an AMD Ryzen 9 5900X 12-Core CPU with 64 GB RAM and a GeForce RTX 3090 24GB GPU. The reported outcomes specifically denote the duration, expressed in milliseconds (ms), that each model required for processing a batch of 20 scans. The retrieval duration was omitted from this experiment because it remains uniform across all models. The size of the models is reported through the count of parameters, denominated in millions (M). PNP GAP emerges as one of the smaller models, comprising 0.4 million parameters and demanding on average 4.4 ms per batch.

A comparative analysis against other SOTA models reveals that PNP GAP has approximately 5% of the size of LOGG3D-Net and is 31 times faster. Furthermore, in comparison to PointNetVLAD, PNP GAP is only 2% of its size and is 6 times faster. These outcomes highlight the computational efficiency of the proposed PNP GAP model.

V. CONCLUSIONS

In this letter, we addressed the 3D LiDAR place recognition problem in horticultural settings by introducing a novel aggregation approach that fuses two statistic-inspired aggregators into a model called PointNetPGAP; an SLC model to handle inter-row descriptor ambiguities; and a novel dataset, HORTO-3DLM, which includes four sequences: three from orchards and one from a strawberry plantation.

The experimental evaluation was conducted on the HORTO-3DLM dataset, and the proposed PointNetPGAP model was benchmarked against SOTA models. An ablation study demonstrated the superiority of the combined aggregators, while the results at both the sequence and segment levels show the proposed model outperforming SOTA models while being more efficient.

Regarding the proposed training approach, all models were trained with and without the SLC model. The results showed that, except for one model, incorporating the SLC model during training led to an increase in performance. This improvement was primarily observed in segments with high inter-row similarity. This suggests that providing a context-specific training signal, as offered by the SLC model, may be crucial for effectively training place recognition models in environments where LiDAR scans overlap significantly, even when originating from different rows.

ACKNOWLEDGMENTS

This work has been supported by the project GreenBotics (ref. PTDC/EEI-ROB/2459/2021), funded by Fundação para a Ciência e a Tecnologia (FCT), Portugal, and by Innovate UK under the Grant No. 10072930 and 10073332. It was also partially supported by FCT through grant UIDB/00048/2020 and under the PhD grant with reference 2021.06492.BD. The authors would also like to thank Dr Charles Whitfield at NIAB East Malling for facilitating orchard data collection campaigns.

REFERENCES

- [1] R. Sparrow and M. Howard, "Robots in agriculture: prospects, impacts, ethics, and policy," *precision agriculture*, vol. 22, pp. 818–833, 2021.
- [2] D. Cattaneo, M. Vaghi, and A. Valada, "LCDNet: Deep Loop Closure Detection and Point Cloud Registration for LiDAR SLAM," *IEEE Transactions on Robotics*, vol. 38, no. 4, pp. 2074–2093, 2022.
- [3] T. Barros, R. Pereira, L. Garrote, C. Premebida, and U. J. Nunes, "Place recognition survey: An update on deep learning approaches," *arXiv preprint arXiv:2106.10458*, 2021.
- [4] T. Barros, L. Garrote, M. Aleksandrov, C. Premebida, and U. J. Nunes, "TRer: A Lightweight Transformer Re-Ranking Approach for 3D LiDAR Place Recognition," in *2023 IEEE 26th International Conference on Intelligent Transportation Systems (ITSC)*. IEEE, 2023.
- [5] J. Guo, P. V. Borges, C. Park, and A. Gawel, "Local Descriptor for Robust Place Recognition using LiDAR Intensity," *IEEE Robotics and Automation Letters*, vol. 4, no. 2, pp. 1470–1477, 2019.
- [6] D. Cheng, F. C. Ojeda, A. Prabhu, X. Liu, A. Zhu, P. C. Green, R. Ehsani, P. Chaudhari, and V. Kumar, "TreeScope: An Agricultural Robotics Dataset for LiDAR-Based Mapping of Trees in Forests and Orchards," *arXiv preprint arXiv:2310.02162*, 2023.
- [7] C. R. Qi, H. Su, K. Mo, and L. J. Guibas, "PointNet: Deep Learning on Point Sets for 3D Classification and Segmentation," in *Proceedings of the IEEE Conference on Computer Vision and Pattern Recognition (CVPR)*, July 2017, pp. 652–660.
- [8] J. Ma, J. Zhang, J. Xu, R. Ai, W. Gu, and X. Chen, "OverlapTransformer: An Efficient and Yaw-Angle-Invariant Transformer Network for LiDAR-Based Place Recognition," *IEEE Robotics and Automation Letters*, vol. 7, no. 3, pp. 6958–6965, 2022.
- [9] M. Angelina Uy and G. Hee Lee, "PointNetVLAD Deep Point Cloud Based Retrieval for Large-Scale Place Recognition," in *Proceedings of the IEEE Conference on Computer Vision and Pattern Recognition (CVPR)*, 2018, pp. 4470–4479.
- [10] K. Vidanapathirana, M. Ramezani, P. Moghadam, S. Sridharan, and C. Fookes, "LoGG3D-Net: Locally Guided Global Descriptor Learning for 3D Place Recognition," in *2022 International Conference on Robotics and Automation (ICRA)*, 2022.
- [11] F. Ou, Y. Li, and Z. Miao, "Place Recognition of Large-Scale Unstructured Orchards with Attention Score Maps," *IEEE Robotics and Automation Letters*, vol. 8, no. 2, pp. 958–965, 2023.
- [12] S. Siva, Z. Nahman, and H. Zhang, "Voxel-Based Representation Learning for Place Recognition Based on 3D Point Clouds," in *2020 IEEE/RSJ International Conference on Intelligent Robots and Systems (IROS)*. IEEE, 2020.
- [13] J. Komorowski, "MinkLoc3D: Point Cloud Based Large-Scale Place Recognition," in *Proceedings of the IEEE/CVF Winter Conference on Applications of Computer Vision (WACV)*, 2021, pp. 1790–1799.
- [14] L. Li, X. Kong, X. Zhao, T. Huang, W. Li, F. Wen, H. Zhang, and Y. Liu, "RINet: Efficient 3D lidar-based place recognition using rotation invariant neural network," *IEEE Robotics and Automation Letters*, vol. 7, no. 2, pp. 4321–4328, 2022.
- [15] T. Barros, L. Garrote, R. Pereira, C. Premebida, and U. J. Nunes, "AttDLNet: Attention-Based Deep Network for 3D LiDAR Place Recognition," in *ROBOT2022: Fifth Iberian Robotics Conference: Advances in Robotics, Volume 1*. Springer, 2022, pp. 309–320.
- [16] S. Shi, C. Guo, L. Jiang, Z. Wang, J. Shi, X. Wang, and H. Li, "PV-RCNN: Point-Voxel Feature Set Abstraction for 3D Object Detection," in *Proceedings of the IEEE/CVF Conference on Computer Vision and Pattern Recognition (CVPR)*, 2020, pp. 10 529–10 538.
- [17] C. Choy, J. Gwak, and S. Savarese, "4D Spatio-Temporal ConvNets: Minkowski Convolutional Neural Networks," in *Proceedings of the IEEE/CVF Conference on Computer Vision and Pattern Recognition (CVPR)*, 2019, pp. 3075–3084.
- [18] C. R. Qi, H. Su, K. Mo, and L. J. Guibas, "PointNet: Deep Learning on Point Sets for 3D Classification and Segmentation," in *Proceedings of the IEEE Conference on Computer Vision and Pattern Recognition (CVPR)*, 2017, pp. 652–660.
- [19] R. Arandjelovic, P. Gronat, A. Torii, T. Pajdla, and J. Sivic, "NetVLAD: CNN Architecture for Weakly Supervised Place Recognition," in *Proceedings of the IEEE Conference on Computer Vision and Pattern Recognition (CVPR)*, 2016, pp. 5297–5307.
- [20] G. Tolias, R. Sicre, and H. Jégou, "Particular object retrieval with integral max-pooling of CNN activations," *arXiv preprint arXiv:1511.05879*, 2015.
- [21] A. Geiger, P. Lenz, and R. Urtasun, "Are we ready for autonomous driving? The KITTI vision benchmark suite," in *2012 IEEE Conference on Computer Vision and Pattern Recognition*, 2012, pp. 3354–3361.
- [22] G. Kim, Y. S. Park, Y. Cho, J. Jeong, and A. Kim, "Mulran: Multimodal range dataset for urban place recognition," in *2020 IEEE International Conference on Robotics and Automation (ICRA)*. IEEE, 2020, pp. 6246–6253.
- [23] W. Maddern, G. Pascoe, C. Linegar, and P. Newman, "1 year, 1000 km: The Oxford RobotCar dataset," *The International Journal of Robotics Research*, vol. 36, no. 1, pp. 3–15, 2017.
- [24] J. Xie, M. Kiefel, M.-T. Sun, and A. Geiger, "Semantic Instance Annotation of Street Scenes by 3D to 2D Label Transfer," in *Proceedings of the IEEE Conference on Computer Vision and Pattern Recognition (CVPR)*, 2016, pp. 3688–3697.
- [25] J. Knights, K. Vidanapathirana, M. Ramezani, S. Sridharan, C. Fookes, and P. Moghadam, "Wild-Places: A Large-Scale Dataset for Lidar Place Recognition in Unstructured Natural Environments," in *2023 IEEE International Conference on Robotics and Automation (ICRA)*. IEEE, 2023.
- [26] P. Jiang, P. Osteen, M. Wigness, and S. Saripalli, "RELLIS-3D Dataset: Data, Benchmarks and Analysis," in *2021 IEEE international conference on robotics and automation (ICRA)*. IEEE, 2021, pp. 1110–1116.
- [27] C. Min, W. Jiang, D. Zhao, J. Xu, L. Xiao, Y. Nie, and B. Dai, "ORFD: A Dataset and Benchmark for Off-Road Freespace Detection," in *2022 International Conference on Robotics and Automation (ICRA)*. IEEE, 2022.
- [28] A. Prabhu, X. Liu, I. Spasojevic, Y. Wu, Y. Shao, D. Ong, J. Lei, P. C. Green, P. Chaudhari, and V. Kumar, "UAVs for forestry: Metric-semantic mapping and diameter estimation with autonomous aerial robots," *Mechanical Systems and Signal Processing*, vol. 208, p. 111050, 2024.